Appendix−Supporting information for:

Engineering a Thermally Localized Janus Membrane for Solar-assisted CO_2 Desorption

Wenqiang Xu[a,b], Qiuhui Xie[a], Yiran Wu[a], Yang Ma[a], Tingting Shu[c*], Ruizhe Wu[a*], Jianjia Yu[d], Lusi Zou[a,e*]

[a] *Hubei Key Laboratory for Precision Synthesis of Small Molecule Pharmaceuticals, College of Chemistry & Chemical Engineering, Hubei University, Wuhan 430062, China*

[b] *School of Materials Science and Engineering, Hubei University, Wuhan 430062, China*

[c] *Normal School, Hubei University, Wuhan 430062, China*

[d] *Department of Chemical Engineering, New Mexico Institute of Mining and Technology, Socorro, NM 87801, USA*

[e] *Hubei Key Laboratory of Novel Reactor and Green Chemical Technology, Wuhan 430062, China*

[*]Corresponding author: Tingting Shu (1019435713@qq.com), Ruizhe Wu (wuruizhe@hubu.edu.cn) and Lusi Zou (lusizou@hubu.edu.cn)

Summary: this file contains 17 pages, 9 Figs, and 3 Tables.

Section 1. Preparation for Various Membranes

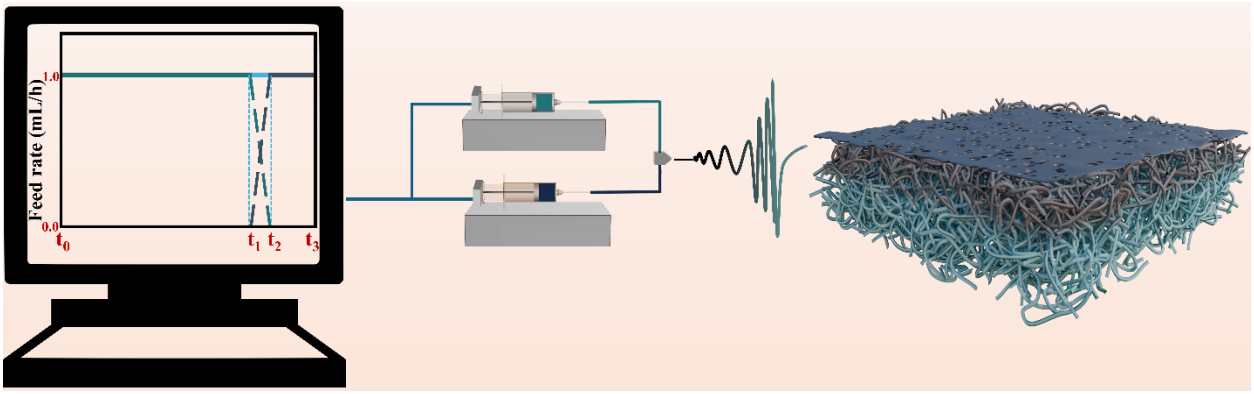

Fig S1. The proposed one-step electrospinning technique for dual-layer substrate fabrication.

All electrospinning membranes were fabricated under identical conditions, with the following parameters: temperature 30 °C, humidity 40%, needle-to-collector distance 12 cm, and an aluminum foil-wrapped roller rotating at 100 rpm as the collector.

Preparation of PVA Electrospinning Nanofiber Membrane

The PVA membrane was fabricated by first dissolving a predetermined amount of PVA in deionized water, followed by magnetic stirring at 500 rpm for 5 hours at room temperature to form a 10 wt% electrospinning solution. Subsequently, a single channel electrospinning strategy was employed. The aforementioned PVA spinning solution was electrospinning at a constant extrusion rate under voltages of 10 kV and -3 kV for a specific period to obtain PVA membranes with corresponding thicknesses. The specific operation times are presented in Table S1.

Crosslinking of PVA nanofiber membrane

Specifically, an aqueous 50 wt% glutaraldehyde solution was diluted to 5 wt% using acetones as a diluent. A catalytic amount of hydrochloric acid was then added to adjust the pH to approximately 1. The pre-prepared PVA nanofiber membrane was fully immersed in this cross-linking solution and subjected to a static reaction at room temperature for 0.5 hours. After the reaction, the cross-linked C-PVA membrane was thoroughly rinsed with deionized water until the effluent pH reached 6.8-7.2, ensuring complete removal of residual glutaraldehyde and reaction by-products from the membrane surface and interior. The cleaned membrane was air-dried at room temperature to yield the final cross-linked C-PVA nanofiber membrane.[1]

Preparation of PVDF Electrospinning Nanofiber Membrane

The PVDF membrane was fabricated by dissolving PVDF powder in a DMF/acetone mixed solvent (6:4 mass ratio) and magnetically stirring the mixture at 500 rpm for 5 hours to form a 10 wt% electrospinning solution. The PVDF spinning solution was subjected to electrospinning using a single channel electrospinning strategy. The electrospinning process was carried out at a constant extrusion rate of 1.0

mL/h, with an applied voltage of 12 kV and - 3 kV, and lasted for 8.0 h. As a result, PVDF membranes with a thickness of 85 μm were successfully obtained.

Preparation of PM Electrospinning Nanofiber Membrane

Firstly, an appropriate amount of PVDF powder was dissolved in the aforementioned TBA-MXene dispersion, and the mixture was magnetically stirred at 500 r/min for 5 hours at room temperature to obtain a homogeneous 3 wt% electrospinning solution. Following the fabrication of the pure PVDF membrane, a subsequent step employed a one-step programmed dual-channel electrospinning process combined with electro spraying. This technique simultaneously processed the PVDF solution and the PVDF/MXene solution under applied voltages of 15 kV and -3 kV to directly fabricate a coherent PVDF-PVDF/MXene multilayer photothermal membrane, which included a transition layer and a supporting layer. Specifically, the PVDF spinning solution was electrospinning alone at a flow rate of 1.0 mL/h for 8 h (corresponding to the time period t_0 - t_1 in Fig S1) to obtain a PVDF membrane with a thickness of 85 μm. Subsequently, a gradient transition layer was prepared using a dual-channel electrospinning setup. The flow rate of the PVDF solution was decreased to 0 over 0.5 h (from t_1 to t_2), while that of the PVDF/MXene solution was increased from 0 to 1.0 mL/h during the same period. Finally, the PVDF/MXene solution was electrospinning at a flow rate of 1.0 mL/h for 2 h (from t_2 to t_3) to form a photothermal layer.

Preparation of PPM Electrospinning Nanofiber Membrane

Firstly, mix the TBA-MXene solution in section 1 with THF at a ratio of 10:1. Add PVDF at 3% wt and PDMS at 2% wt of the TBA-MXene solution to it, heat to 60 °C and stir for 24 hours to obtain a spray solution with a ratio of PVDF: PDMS: MXene = 3: 5: 2. Following the fabrication of the pure PVDF membrane, a subsequent step employed a one-step programmed dual-channel electrospinning process combined with electro spraying. This technique simultaneously processed the PVDF solution and the PVDF/PDMS/MXene solution under applied voltages of 15 kV and -3 kV to directly fabricate a coherent PVDF-PVDF/PDMS/MXene multilayer photothermal membrane, which included a transition layer and a supporting layer. Specifically, the PVDF spinning solution was electrospinning alone at a flow rate of 1.0 mL/h for 8 h (corresponding to the time period t_0 - t_1 in Fig S1) to obtain a PVDF membrane with a thickness of 85 μm. Subsequently, a gradient transition layer was prepared using a dual-channel electrospinning setup. The flow rate of the PVDF solution was decreased to 0 over 0.5 h (from t_1 to t_2), while that of the PVDF/PDMS/MXene solution was increased from 0 to 1.0 mL/h during the same period. Finally, the PVDF/PDMS/MXene solution was electrospinning at a flow rate of 1.0 mL/h for 2 h (from t_2 to t_3) to form a photothermal layer.

Preparation of PPM/C-PVA Electrospinning Nanofiber Membrane

As illustrated in Fig 1, we first fabricated a series of PVA electrospinning membranes with 10 μm using an aqueous PVA solution. The membranes were subsequently crosslinked via an established methodology to

form C-PVA substrates. Using a programmed dual-channel sequential electrospinning strategy, we constructed a photothermal multilayer on the C-PVA support in a consecutive step with PVDF and PVDF/PDMS/MXene solutions. The resulting structure comprised a 2 μm MXene-based photothermal layer, a 3 μm transition layer and an 85 μm PVDF supporting layer, with no discernible delamination. This specific thickness configuration was chosen based on our prior work demonstrating its exceptional photothermal performance. The final membrane was denoted as PPM.

Table S1. Parameters for the electrospinning process: flow rate and duration for each layer.

Membrane Code	Thickness (μm)	Extrusion rate of PVA dope (mL/h)	Extrusion rate of silution (mL/h)	Extrusion rate of PVDF solution dope (mL/h)	Electro-spinning time (h)
PVA layer	5	1.0	-	-	0.25
PVA layer	10	1.0	-	-	0.5
PVA layer	15	1.0	-	-	1.25
PVA layer	20	1.0	-	-	1.0
PVA layer	40	1.0	-	-	2.0
PVA layer	60	1.0	-	-	3.0
PVDF layer	85	-	-	1.0	8.0
Transitional layer	3	-	1.0→0	0→1.0	0.5
Photothermal layer	2	-	1.0	-	2.0

Section 2. Membrane Characteristics

Overall Porosity

The dry membrane sample was first weighed using an analytical balance. The sample was then fully immersed in kerosene for 24 hours to ensure complete wetting. After removal, excess kerosene on the surface was gently wiped off with filter paper, and the weight of the wet membrane was measured. The overall porosity (ε) was calculated by equation (1).[2]

$$\varepsilon = \frac{\frac{\omega_2 - \omega_1}{\rho_{oil}}}{\frac{\omega_2 - \omega_1}{\rho_{oil}} + \frac{\omega_1}{\rho_{mem}}} \quad (1)$$

Where ω_1 and ω_2 represent the mass of the dry and wet membrane, respectively; ρ_{oil} is the density of kerosene (0.8 g/cm^3); and ρ_{mem} denotes the density of the membrane material (1.78 g/cm^3 for PVDF, 1.3 g/cm^3 for PVA). To ensure accuracy, the measurement was repeated five times for each sample, and the average value was reported.

Effective Porosity

The electrospinning membrane was assembled in the middle of the module. N_2 was supplied to one side, while a flowmeter was connected to the other to measure the gas flow rate. The volumetric flow rate was recorded under different feed pressures, and the permeability test was repeated three times at each pressure. The average value of these three measurements was used to calculate the gas permeability. The relationship between gas permeability and average pressure was then plotted, with gas permeability as the ordinate and average pressure as the abscissa. From the linear fit of the data, the intercept and slope (S_0) were obtained.[3] The effective porosity (ε_e) can be calculated using the following equation:

$$\varepsilon_e = \frac{32\mu RT}{d_a^2} S_0 \quad (2)$$

Liquid Entry Pressure (LEP)

The membrane was loaded into a custom module (Fig S2). Deionized water was circulated on the permeate side, and its conductivity was monitored in real-time. The feed side was connected to a tank containing a 3.5 wt% NaCl solution. N_2 was continuously introduced into the tank, and the pressure was gradually increased at a rate of 0.05 bar/min. The LEP was recorded as the pressure gauge reading at the moment a sharp increase in conductivity was detected.

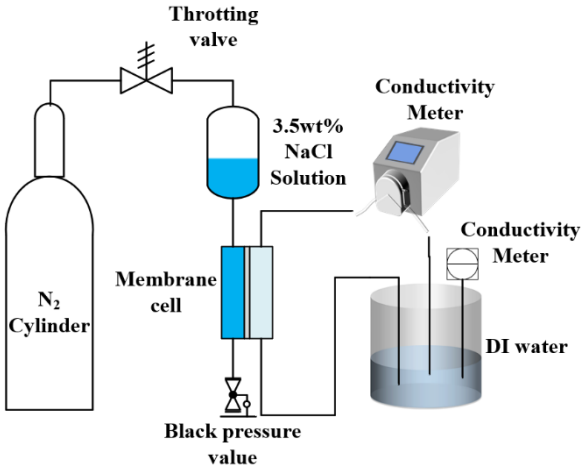

Fig S2. Membrane parameter test device.

Section 3. Photothermal Experiment

Thermal Insulation Testing

The thermal localization effect of the composite membrane was evaluated using a custom membrane reactor. The membrane contactor, a key component fabricated from PTFE, is shown in Fig 2(a). It features a central circular opening 5 cm in diameter sealed with quartz glass and is divided into two compartments: a liquid-side cavity with a height of 2 mm and a gas-side cavity with a height of 1 cm. The membrane was installed between these two compartments, allowing simulated sunlight to pass vertically and uniformly through the quartz glass, thereby providing a stable light field for the photothermal process. The solar simulator, equipped with a standard AM 1.5G filter, provides adjustable irradiance from 0 to 3 kW m^{-2} and a spot diameter ranging from 30 to 50 mm. The irradiance was calibrated prior to experiments using a solar power meter. The temperatures of the membrane surface and the liquid were measured by an infrared thermal camera and the temperature probe, respectively. Prior to testing, the transmittance of C-PVA layers with different thicknesses was measured. The irradiance of the simulated sunlight was adjusted to maintain a constant theoretical maximum temperature of the PM layer after its transmission through the wetted C-PVA layer. The membrane was then installed between the two cavities. Under static water conditions, deionized water was introduced into the reactor until it was completely filled and sealed. Then it was irradiated using a solar simulator with an intensity of 1 kW m^{-2}. The temperature at the top of the water column (2 mm above the membrane surface) was monitored for 10 minutes. Under flowing water conditions, deionized water was continuously pumped through reactor at a flow rate of 4 mL min^{-1} under 1 kW m^{-2} irradiation, the residence time was maintained at 1 minute, and the temperature of the outlet water was recorded.

When the temperature rises to maximum, the system reaches balanced. The sensible heat (Q_{sen}) for water temperature rise can be calculated as follow equation.[4]

$$Q_{sen} = m * C_P * \Delta T \quad (3)$$

Preparation of CO_2-rich AAS Solvent

Based on the mass composition of soybean-based amino acids listed in Table S4, 3 mol of a mixture comprising 18 amino acid powders were weighed and placed into a narrow-necked flask.[5] An equimolar amount of potassium hydroxide was added for neutralization. The mixture was then prepared into an aqueous amino acid salts solution under constant temperature conditions at 20 °C, with continuous cooling to maintain thermal stability, and finally diluted to the specified volume. The pH of the final solution was approximately 12. In calculating the concentration of AAS, the volume contribution from water generated in the neutralization reaction was accounted for. The prepared AAS solvent was heated to 40 °C in a water bath under continuous stirring. A certain amount of pure CO_2 was introduced into the solvent via a gas mass flow controller. The quantification of CO_2 loading was performed through acid-base titration with gasometrical validation. Specifically, an excess of dilute hydrochloric acid was gradually added to a

measured volume of absorption liquid containing methyl orange indicator until a persistent red coloration was observed, confirming complete decomposition of CO_2-absorbed species including carbamate (NH_2COO^-) and bicarbonate (HCO_3^-). The CO_2 loading capacity was subsequently calculated by stoichiometric analysis of the liberated carbon dioxide, with the gas evolution volume being converted to molar quantity using ideal gas law principles under standardized temperature and pressure conditions.[5]

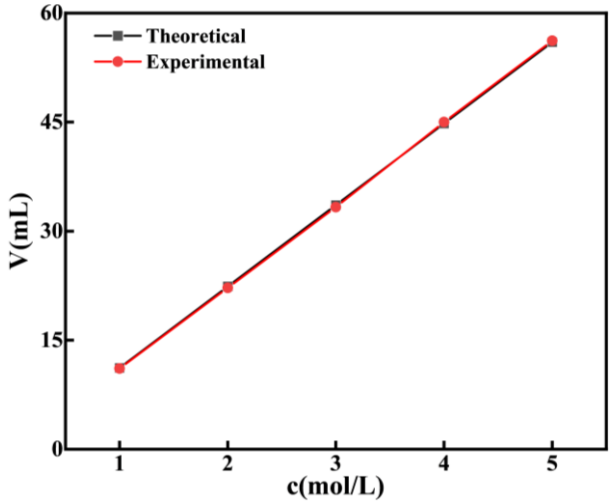

Fig S3. Calibration curve of gas metering device.

Table S2. Components, structure, fraction of amino acids in AAS solution.[5]

Components	Structure	Molar fraction (mol%)	Mass fraction (wt%)
L-Alanine (Ala)	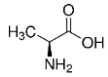	6.41	4.33
L-Arginine (Arg)	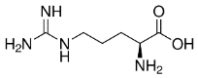	5.81	7.69
Asparticacid (Asp)	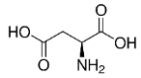	11.48	11.49
L- Cystine (Cys)	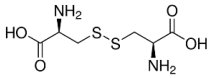	0.93	1.72
L-Glutamicacid (Glu)	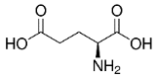	16.61	18.43
Glycine (Gly)	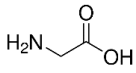	7.52	4.25
L-Histidine (His)	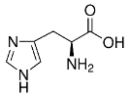	2.36	2.76
L-Isoleucine (Iso)	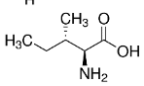	4.72	4.70
L-Leucine (Leu)	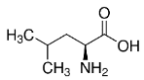	7.93	7.91

Components	Structure	Molar fraction (mol%)	Mass fraction (wt%)
L-Lysine (Lys)	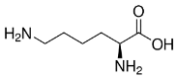	5.87	6.57
L-Methionine (Meth)	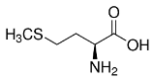	1.30	1.49
L-Phenylalanine (Phe)	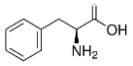	4.17	5.22
L-Proline (Pro)	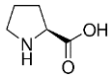	5.65	4.93
L-Serine (Ser)	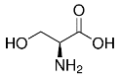	5.83	4.63
L-Threonine (Thr)	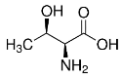	4.34	3.96
L-Tryptophan (Try)	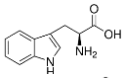	0.78	1.19
L-Tyrosine (Tyr)	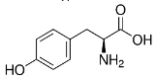	2.69	3.73
L-Valine (val)	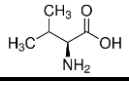	5.59	5.00

Solar-assisted CO_2 Desorption Experiment

This study employed a custom-built, solar-driven CO_2 desorption setup to investigate the regeneration efficiency of the amino acid-based solvents, as illustrated in Fig 3(b). The system primarily consists of a xenon light solar simulator, a peristaltic pump, a gas mass flow controller and a CO_2 infrared analyzer. For fluid handling, the CO_2-rich solvent and N_2 gas were circulated counter currently flow on opposite sides of the membrane. The liquid flowed through a 2-mm-high channel to minimize heat transfer to the bulk solution, while the gas passed through a 1-cm-high cavity to ensure complete mixing of the desorbed CO_2 with the N_2 stream. This configuration stabilized the outlet CO_2 concentration, which enhanced measurement accuracy and reliability. During operation, the xenon lamp was maintained at a vertical distance of over 30 cm from the contactor to minimize heating from source radiation. The outlet CO_2 concentration was monitored in real time using the infrared analyzer. Temperatures at the absorber surface, within fluid channels, and of the ambient environment were recorded by a multi-channel temperature logger once readings stabilized. Simultaneously, the temperature distribution across the absorber surface was captured using an infrared thermal imager positioned at a 60° angle and approximately 30 cm from the sample. The regeneration performance of CO_2-rich solvent was evaluated using follow equations.[6]

CO_2 desorption flux, J_{CO_2} (mmol m^{-2} s^{-1})

$$J_{CO_2} = \frac{dM_{CO_2} \times Q}{A} \tag{4}$$

Where Q is the solvent flow ($m^3\ s^{-1}$), A is the gas-liquid contact area (m^2), and dM_{CO_2} is the difference of the CO_2 concentration (mol L^{-1}) between inlet and outlet.

CO_2 regeneration efficiency, η (%)

$$\eta = \frac{M_{CO_2}\big|_{t=0} - M_{CO_2}\big|_{t=t}}{M_{CO_2}\big|_{t=0}} \times 100\% \quad (5)$$

Where M_{CO_2} is the CO_2 concentration (mol L^{-1}) in the solvent and t is the regeneration time.

Specific regeneration energy (thermal energy input for absorbent heating only), Q_R (GJ ton^{-1} of CO_2 released)

$$Q_R = \frac{Q_{heat}}{M_{CO_2}\big|_{t=0} - M_{CO_2}\big|_{t=t}} \frac{1}{V_s MW_{CO_2}} \quad (6)$$

Where Q_{heat} is the heat energy for the regeneration process (GJ), MW_{CO_2} is CO_2 molecular weight (44.01 g mol^{-1}), and V_s is the solvent volume (L).

Section 4. PVA Membrane Analysis

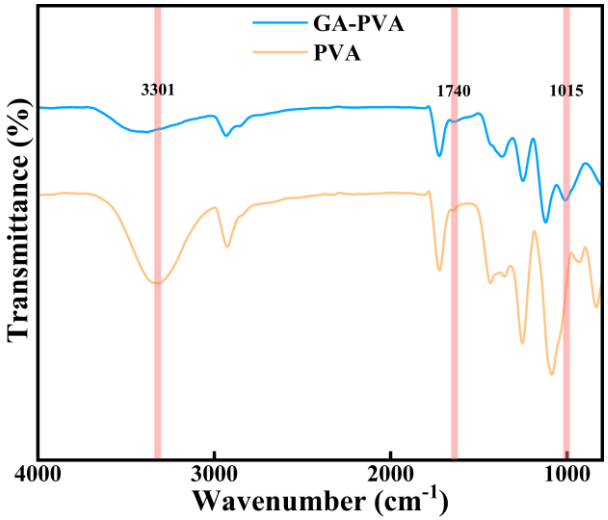

Fig S4. FTIR spectra of the PVA membrane before and after cross-linking.

Section 5. Characterization of $Ti_3C_2T_X$ MXene

The MAX phase (Fig S5(a)) was selectively etched with hydrofluoric acid to obtain multilayer MXene (Fig S5(b)). Subsequently, TBAOH was used as an intercalant and surface modifier to convert it into TBA-$Ti_3C_2T_X$ powder. As shown in Fig. S5(c) and (d), the intercalated TBA-MXene exhibits a relatively large size distribution with an average size of 1.2 μm.

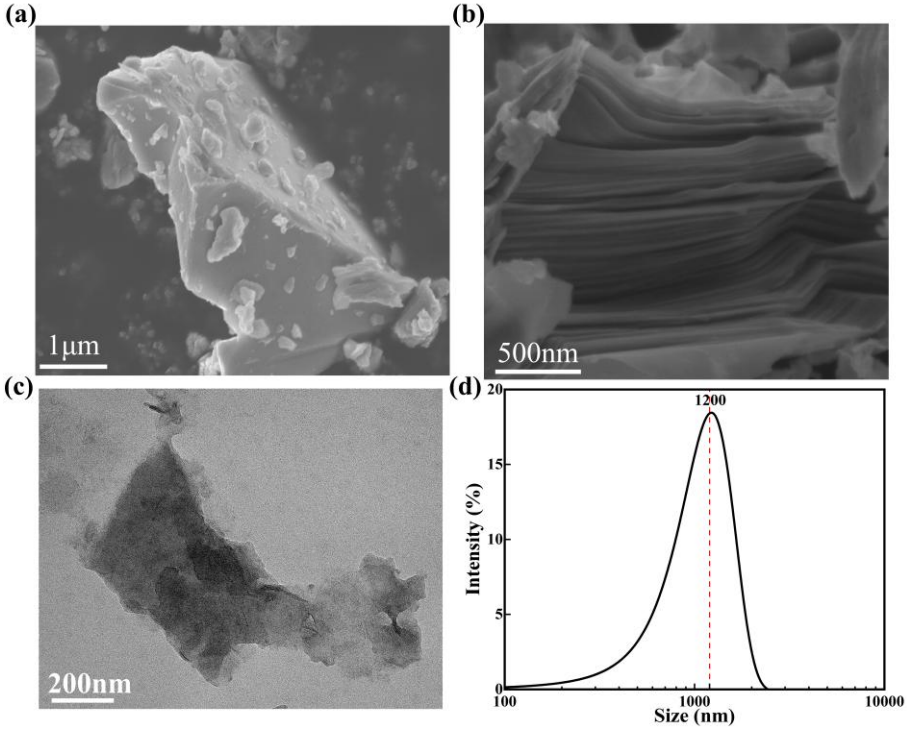

Fig S5. (a) FESEM image of MAX phase precursor; (b) FESEM image of the HF-etched MAX phase;

(c) FESEM image of the resultant MXene; (d) Lateral size distribution of the MXene nanosheets.

The structural evolution of MXene upon intercalation was investigated by X-ray diffraction (XRD). As shown in Fig S6(a), the (002) diffraction peak of the pristine MXene agreed well with reported values, confirming the successful preparation of the baseline material. After intercalation with TBAOH, the (002) peak of the TBA-MXene sample shifted by 0.9° to a lower angle (from 8.2°), which signifies a significant expansion of the interlayer spacing and provides direct evidence for the successful insertion of TBA^+ ions. Moreover, the chemical composition and bonding states of the MXene nanosheets were probed by X-ray photoelectron spectroscopy (XPS). The survey spectrum in Fig S6(b) confirmed the presence of Ti, C, O, and F, while a comparative analysis revealed a significantly higher N content in TBA-MXene than in pristine $Ti_3C_2T_X$. This marked increase in nitrogen unequivocally demonstrates the successful intercalation of TBA^+ ions, which partially replaced the surface -OH groups. This substitution is critical for enhancing the material's oxidation resistance.[7]

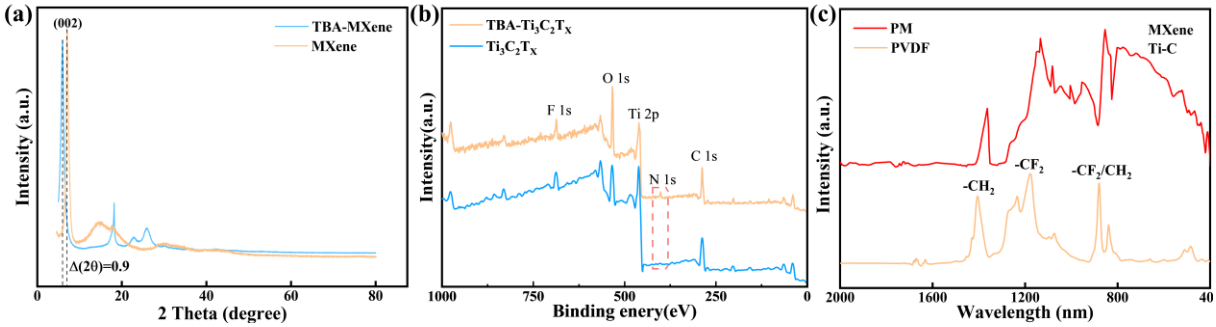

Fig S6. (a) XRD patterns of pristine and TBA-intercalated MXene; (b) XPS survey spectra of the corresponding MXene sheets; (c) FTIR spectra of the PVDF and PM membranes.

Section 6. Long term testing and PPM/C-PVA membrane characteristics

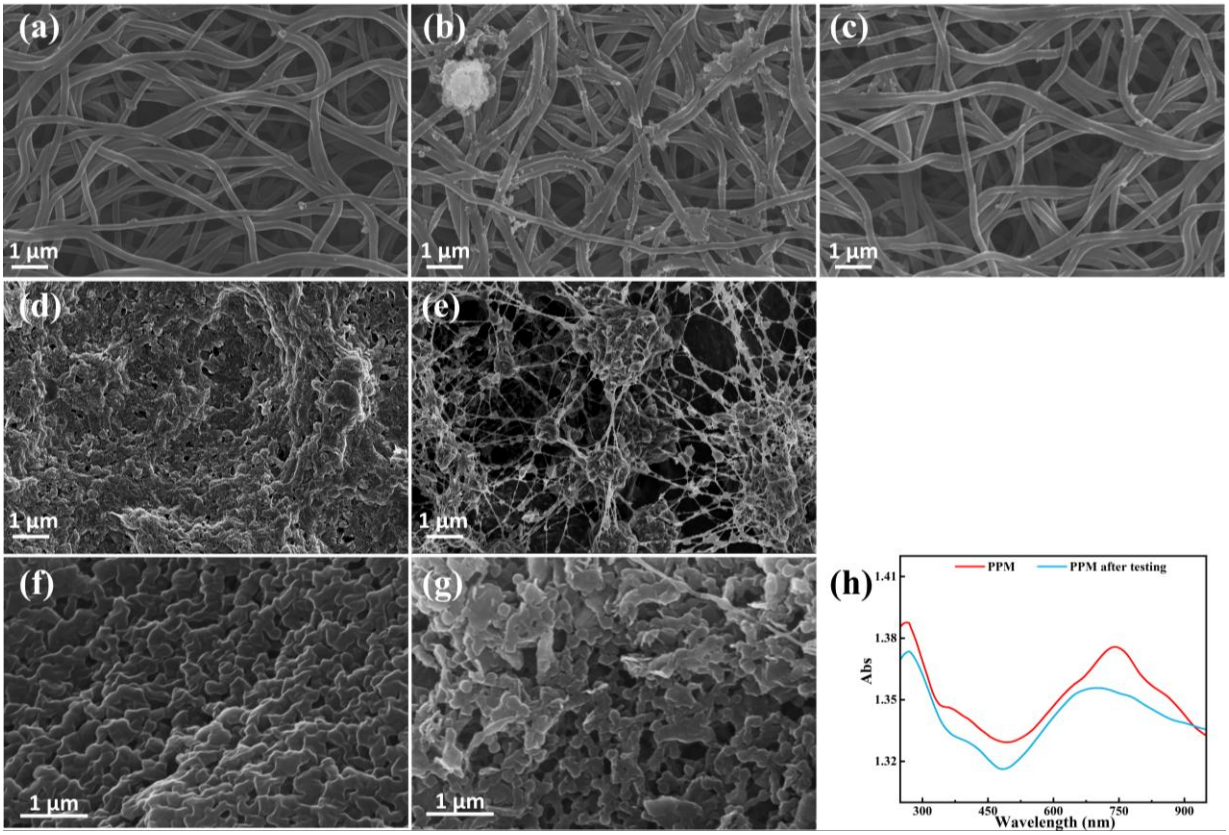

Fig S7. FESEM characterization of the membrane structures: (a-c) the C-PVA membrane before operation, after long-term operation, and after cleaning; (d,e) the PM membrane photothermal layer before and after the long-term operation; (f,g) the PPM membrane photothermal layer before and after the long-term operation; (h) absorbance spectra of PPM membrane.

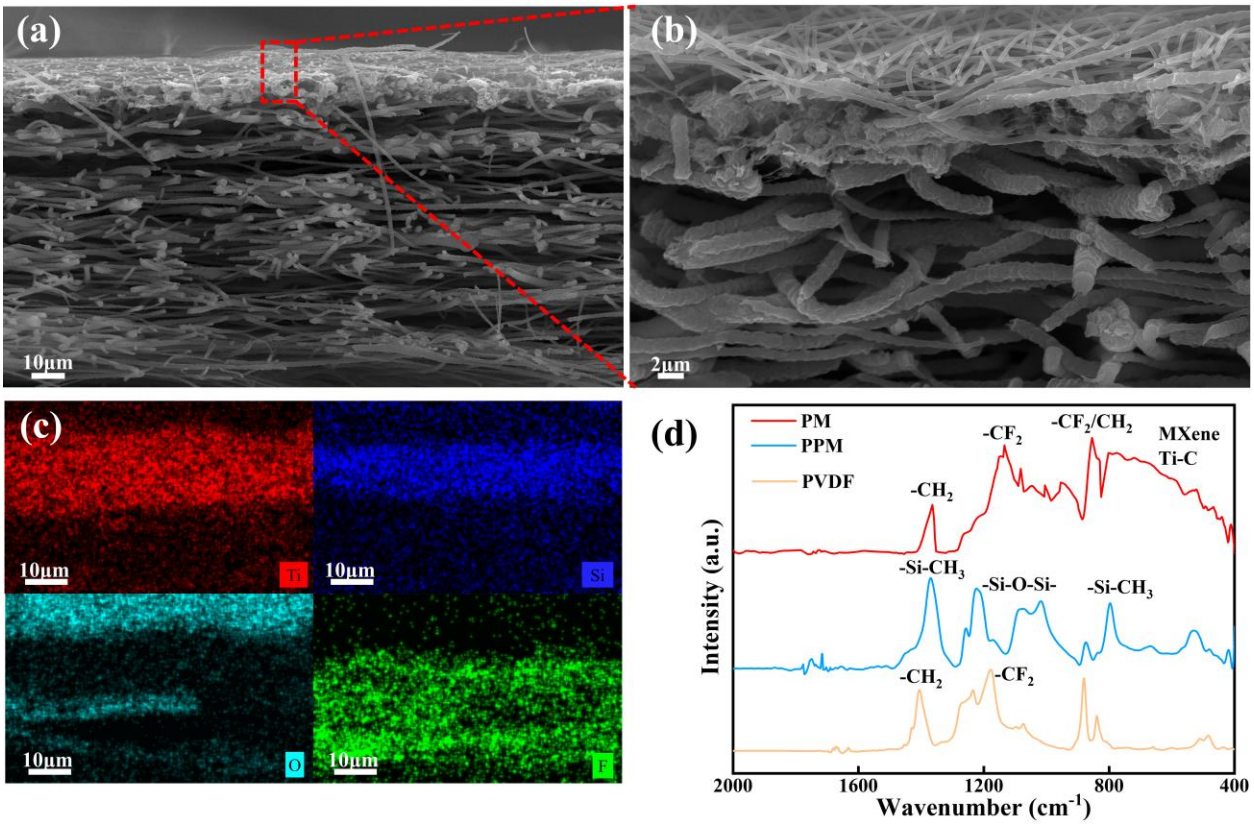

Fig S8. (a) cross-section view of PPM/C-PVA membrane; (b) magnified view of the cross-section joint; (c) elemental mapping confirming the material distribution of the magnified view; (d) FTIR spectra of different membranes.

Table S3. Pore characteristics of different membrane.

Membrane Code	Thickness (L, μm)	Overall Porosity (ε, %)	Effective Porosity (ε_e, m^{-1})	Maximum Pore size (d_m, μm)	Average Pore size (d_a, μm)	Gas Permeability ($m^3\ m^{-2}\ bar^{-1}\ s^{-1}$)	LEP (kPa)
PPM	90	86 ± 0.6	17684.15	1.12	0.25	2.98	160±5
PPM/C-PVA	100	88 ± 1.1	15948.01	1.15	0.26	2.89	170±5

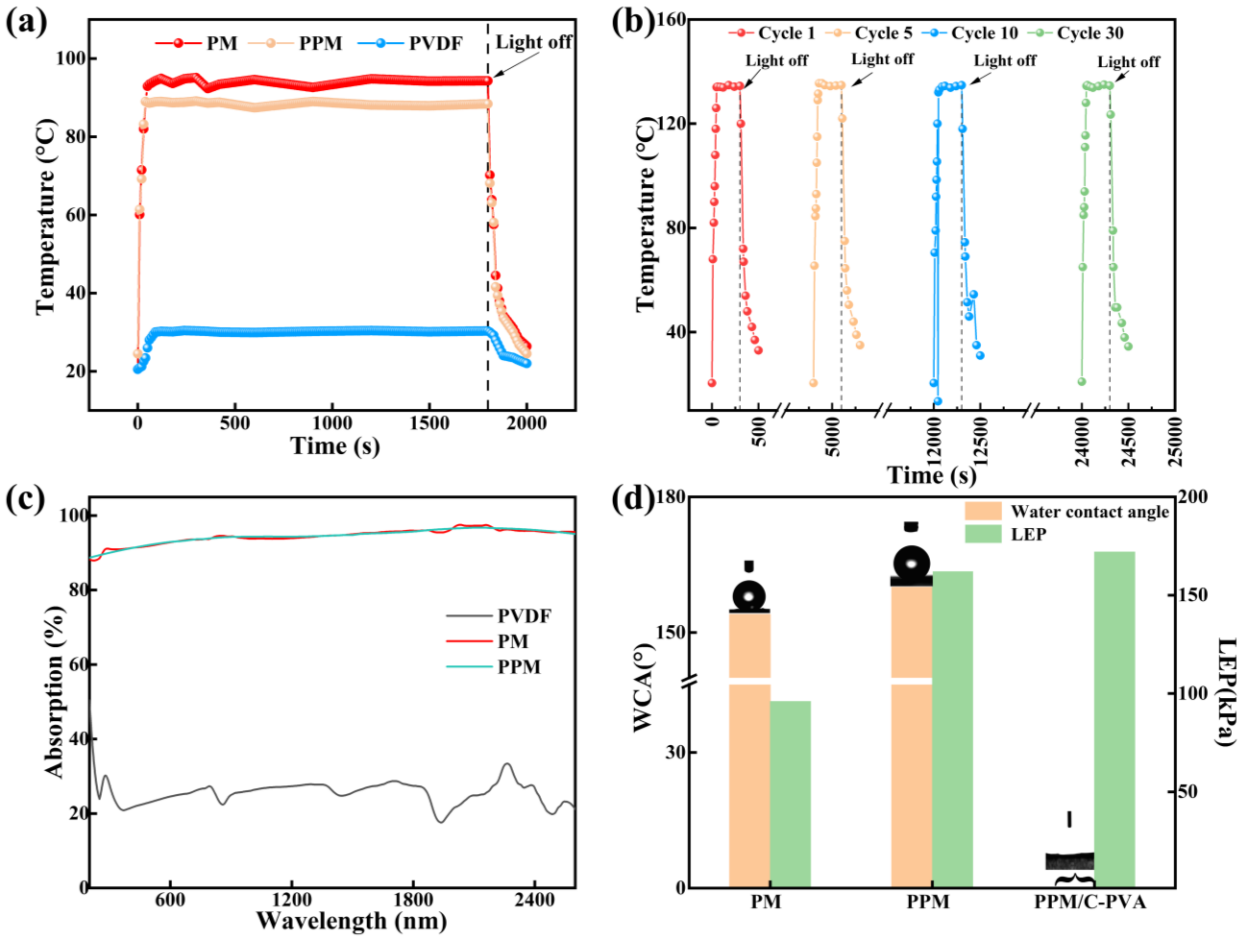

Fig S9. (a)Temperature change as a function of time for membrane under 1 kW m^{-2} illumination; (b)Temperature change as cycles of light up/off for PPM membrane under 3 kW m^{-2} illumination; (c) Optical absorbance spectra of different membranes; (d) Liquid entry pressure and water contact angle of various membranes.

Section 7. Technoeconomic analysis

A technoeconomic analysis was conducted to evaluate the feasibility of the carbon capture system, with calculations based on experimentally validated parameters. The analysis considered a system designed for a CO_2 capture capacity of 1 million tons annually.

System Parameters and Cost

The carbon capture system is scaled up based on lab-scale continuous-flow experimental results. The CO_2-rich solution is pumped through a membrane contactor into a heating chamber, powered by electric heating (or waste heat) and solar heating. The width of the membrane is 100 cm, the length of the membrane inside the heating chamber is 200 cm, corresponding to a heating chamber volume of 0.1 m^3 (the liquid height is 5 cm). Based on lab-scale experiments, the flow speed is set for the sorbent solution to stay in the heating chamber for specific min to achieve 50% desorption. The volume of sorbent solution flowed per hour is:

$$Q_L = \frac{\text{heating chamber volume}}{Retain\ time} \quad (7)$$

The CO_2 amount captured per volume of liquid flowed through the heating chamber is set to be ~ 2.4 mol per liter based on our experimental results. To meet the annual carbon capture capacity of 10 thousand tons, the number of membranes needed for the whole system is:

$$n = \frac{\text{annual capability}}{44g/mol \times volumetric\ capacity \times 365 \times 24} \quad (8)$$

The chemicals cost consists of the costs of AAS, with a unit price of 2 $/kg. According to the current composite membrane preparation process in our laboratory, each square meter of membrane requires approximately 8 g of PVDF (10 wt%), 0.2 g of PVA, 0.6 g of MXene, and 0.2 g of PDMS, with a production cost of about $3/m^2 (based on an MXene cost of $3.3/g).[8] Assuming the membrane can operate continuously for 10 days with less than 20% loss, and considering a system lifetime of 25 years and a capital recovery factor of 8.2% due to material consumption and system maintenance over time, the annual system cost is calculated as follow[9]:

$$System\ cost = \frac{n \times (chemicals\ cost + membrane\ cost)}{25} + n \times (chemicals\ cost + membrane\ cost) * 0.082 \quad (9)$$

Under the current experimental conditions, the system uses waste heat as the heat source in the temperature range of 40 – 60 °C, and uses natural gas for heating in range the of 60.1 – 90 °C. The relevant economic parameters are set as follows: the price of natural gas is $0.3 per cubic meter, the heating efficiency of natural gas is 85%, the electricity cost is $0.07 per kWh, and the cost of waste heat is $0.02 per kWh.[10] The Pumping cost at specific operational conditions can be calculated by:

$$Pumping\ cost = Pumping\ energy * 0.07/277.8 \quad (10)$$

The Heating cost at specific operational conditions (>60 °C) can be calculated by:

$$Heating\ cost = Heating\ energy * 0.03/0.0353 \quad (11)$$

The Heating cost at specific operational conditions (>60 °C) can be calculated by:

$$Heating\ cost = Heating\ energy * 0.02/277.8 \quad (12)$$

The total cost at specific operational conditions can be calculated by:

$$Total\ cost = System\ cost + Pumping\ cost + Heating\ cost \quad (13)$$

REFERENCES

1. A. Barlybayeva, B. Myrzakhmetov, Y. Wang and A. Mentbayeva, *Sci. Rep.*, 2024, **14**, 25603.
2. L. Zou, P. Gusnawan, G. Zhang and J. Yu, *J. Membr. Sci*, 2020, **615**, 118552.
3. M. Khayet and T. Matsuura, in Membrane Distillation, eds. M. Khayet and T. Matsuura, Elsevier, 2011; pp 1-16.
4. L. Zhang, B. Bai, N. Hu and H. Wang, Sol. *Energy Mater. Sol. Cells,* 2021, **221**, 110876.
5. W. Xu, P. Liu, L. Hu, Y. Zhang, P. J. Gusnawan, J. Yu and L. Zou, *Sep. Purif. Technol*, 2025, **376**, 133872.
6. P. J. Gusnawan, L. Zou, G. Zhang and J. Yu, *ACS Sustainable Chem. Eng.*, 2020, **8**, 3929-3937.
7. Q. Zhang, H. Lai, R. Fan, P. Ji, X. Fu and H. Li, *ACS Nano*, 2021, **15**, 5249-5262.
8. J. Serafin, S. Chaitoglou, G. Farid, Y. Ma, B. Dziejarski, A. Sanchez, X. Vendrell and R. Amade, *Chem. Eng. J.*, 2025, **523**, 168650.
9. Y. Guo and T. A. Hatton, *Nat. Chem. Eng*, 2025, **3**, 70-78.
10. E. Taibi, D. Gielen and M. Bazilian, *Renew Sust Energ Rev*, 2012, **16**, 735-744.